CHEMPHYSCHEM

Supporting Information

Three-Dimensional Super-Resolution Imaging of the Midplane Protein FtsZ in Live *Caulobacter crescentus* Cells Using Astigmatism

Julie S. Biteen,[a, b] Erin D. Goley,[c, d] Lucy Shapiro,[c] and W. E. Moerner*[a]

cphc_201100686_sm_miscellaneous_information.pdf
cphc_201100686_sm_1.avi
cphc_201100686_sm_2.avi

Contents:

Movies:

1. **FtsZ Live and Fixed_20nmBlob_400nmScaleBar.avi**

   360° view of the FtsZ structures corresponding to Figures 3 – 6 of the main text. Here, each localization is represented as a 2D Gaussian with intensity proportional to total number of photons collected and with a uniform width of 20 nm. Scale bar, 400 nm.

2. **FtsZ Live and Fixed_1nmSpot_400nmScaleBar.avi**

   360° view of the FtsZ structures corresponding to Figures 3 – 6 of the main text. Here, each localization is represented as a 1-nm radius spot with uniform intensity. Scale bar, 400 nm.

Supplementary Methods

Sample preparation

A gene encoding a xylose-inducible, Dendra2 (Clontech) fluorescent protein fusion to the midplane protein FtsZ was introduced in single copy into the chromosome of *C. crescentus* to permit control of the expression level of the C-terminal FtsZ-Dendra2 construct. Cells were grown initially in PYE rich media at 28 °C and then diluted into M2G minimal media for 24 h. After a 1-h incubation in 0.015 % xylose, cells were concentrated by centrifugation. For live-cell samples, 5 μL of the concentrated cells resuspended in M2G were added directly to a pad of 1.5% agarose in M2G on a coverslip with 1 μL of TetraSpeck™ fluorescent microspheres (Invitrogen Molecular Probes) which served as fiduciary markers. Cell viability was assessed by observation of cell division for a majority of the cells. For the fixed-cell samples, cells were incubated in 135 μL 37% formaldehyde per 5 mL culture for 40 min and washed in minimal media three times, and then 5 μL of the fixed cells were added to a 1.5% agarose pad on a coverslip with 1 μL of TetraSpeck™ fluorescent microspheres. All samples were covered with a second coverslip and sealed with paraffin wax to prevent drying, and imaged within 1.5 h of preparation.

Imaging

Both white-light transmission cellular images and epifluorescence images of single molecules in the cellular samples were acquired with an Olympus IX71 inverted microscope fitted with a 1.41-NA oil immersion objective and detected on a 512 × 512 pixel Andor Ixon EMCCD at a rate of 15 ms/frame. The general epifluorescence setup is as previously described;[1, 2] here we used a dichroic filter (Semrock Di-01-561), a long-pass filter (Semrock BLP01-561R), a 561-nm diode-pumped solid-state laser (Crystalaser CL561-025-O) for imaging, and a 407-nm laser (Coherent Innova 300 Kr^+ laser) for photoswitching. For the 3D astigmatic acquisitions, a 1-m focal length cylindrical lens was placed in the microscope emission pathway, 2.0 cm before the usual imaging plane, and the camera position was adjusted for focus.

Dendra2 is a green-to-red photoswitchable fluorescent protein.[3] Initially non-activated, the Dendra2 molecules expressed in our *C. crescentus* cells began in their green state and were not visible under 561-nm laser illumination. A subset of Dendra2 molecules were activated (switched to the red state) by illumination at 407 nm. The 407-nm activation fluence of ~10^3 W/cm^2 for 0.1-0.5 s was chosen so that at most one Dendra2 molecule was visible in each diffraction-limited region (1-2 Dendra2 molecules in any given Z-ring). The sample was then imaged with 561-nm excitation at ~10^3 W/cm^2 with a 15-ms integration time per frame.

For the live-cell samples, soluble, cytoplasmic FtsZ-Dendra2 fusions were not resolvable due to their rapid diffusion during our 66.7 frames per second imaging speed, and only single molecules of FtsZ-Dendra2 incorporated into protofilaments in the Z-ring were slowed enough to appear as punctate spots in 15-ms frames. This led to an effective blinking in our data: “visible” when an FtsZ-Dendra2 molecule became polymerized (and was resolved by the camera) and “invisible” when the molecule bleached or depolymerized, as discussed below. For these samples, a new subset of red FtsZ-Dendra2 molecules needed to be activated (with a 0.5-s 407-nm laser pulse) only every 10 s.

For the fixed-cell samples, all FtsZ-Dendra2 molecules appeared as punctate spots since all were immobilized and the only photoswitching in the data is attributed to photoactivation (to the "on" state) and photobleaching (to the "off" state). In order to activate only one Dendra2 per diffraction-limited region, fewer Dendra2 could be activated at any one time, and cycles of photoactivation (with a 0.1-s 407-nm laser pulse), imaging, and photobleaching were repeated every 2 s.

Peak fitting, statistical localization precision in *x* and *y*, and *z* position determination

For each imaging frame, each isolated localized single-molecule spot, a representation of the microscope point-spread-function, $I(x,y)$, was fit to an asymmetric 2D Gaussian function,

$$I(x,y) = B + A\exp\left(-\frac{(x-x_0)^2}{2\sigma_x^{\,2}} - \frac{(y-y_0)^2}{2\sigma_y^{\,2}}\right)$$

where B is the background fluorescence, A is the amplitude, (x_0 , y_0) is the peak position, and σ_x and σ_y are the standard deviations in the x and y dimensions, respectively. The fit was obtained using the MATLAB nonlinear least squares regression function, nlinfit. To compensate for stage drift during imaging, the positions of the FtsZ-Dendra2 molecules were determined relative to the positions of fixed fiduciaries (TetraSpeck™ fluorescent microspheres) in the same field of view. The center position (x_0 , y_0) indicates the in-plane position of each molecule, and the statistical precision of this localization was given by the half-width 95% confidence interval for this position from the fit. Only molecules with $\leq$ 30 nm statistical localization precision in x and y were considered in reconstructing the output image. For the 2D image in Figure 2 in the main text, only molecules where the fit yielded a nearly symmetric Gaussian ($0.67 < \sigma_x/\sigma_y < 1.5$) were considered. Each well-fit molecule was plotted as a Gaussian profile with fixed standard deviation, σ = 30 nm, and with amplitude proportional to the inverse of the localization precision of that molecule

In 3D experiments, the cylindrical lens introduces astigmatism in the image, and the resulting degree of asymmetry is used to determine the z position of each localized molecule. The system is calibrated using a sample consisting of a fiduciary marker on a glass coverslip; this sample is translated along the z axis with a piezo objective positioner (PIFOC, Physik Instrumente) having nm-scale precision. The PSF at each known z position is fit with an asymmetric Gaussian, and the ratio σ_x/σ_y recorded. This curve is fit to an analytical defocusing equation,[4]

$$\frac{\sigma_x}{\sigma_y}(z) = \frac{\sqrt{1+\left(\frac{z-c_x}{d}\right)^2}}{\sqrt{1+\left(\frac{z-c_y}{d}\right)^2}}$$

where d is the focus depth, c_x is the x focal plane offset, and c_y is the y focal plane offset.

Since the calibration sample emission is transmitted through only the glass coverslip and index-matching objective oil while the real samples are in an aqueous environment, the effect of defocusing is affected by

the difference in refractive index. The *z* position of the fluorophores in the FtsZ-Dendra2 experiments in this work were therefore obtained by determining *z* from the measured σ_x/σ_y ratio according to the fiduciary calibration, and then multiplying this value by 1.33/1.51 (the ratio of the refractive indices of water and glass).[5]

Estimation of the localization precision in *x*, *y*, and *z* by sequential localizations

The transverse statistical localization precision of each single-molecule fit was determined based on the 95% confidence interval in (*x,y*) position as given by the Matlab routine nlinfit, as described above. Since most molecules were imaged for more than one frame, the localization precision could also be determined from successive fits of the same molecule. When a molecule was localized three or more times in consecutive frames within the same diffraction-limited region, the standard deviation of the resulting positions (*x,y,z*) for each fit was calculated. The results for the live stalked cell in Figure 3 in the main text are plotted in Figure S1.

Importantly, the localization precision in *x* and *y* agrees well with the statistical localization precision described above; all fits have a standard deviation less than 30 nm in *x* and *y*. This method additionally permits an estimation of the precision in *z*, which could not be easily obtained from the peak-fitting algorithm alone. The *z* precision is less than 100 nm for all the points that are considered.

Finally, a correlation between the *z* position and the localization precisions is also observed in the scatter plots above. As discussed in Badieirostami et al., the localization precision in these astigmatic imaging techniques is a function of the emitter depth, and is best near the focus.[6] In the figure above, we observe the lowest values of σ_x, σ_y and σ_z near the focal plane of the sample (at z = 612 nm). Badieirostami et al. find 15-20 nm error in *z* in simulations of astigmatic imaging for 1000 photons detected; here the errors are greater mostly due to the considerably smaller signal (50-200 photons detected per localization) and also to the slightly higher background observed here (3-5 photons/pixel/frame).

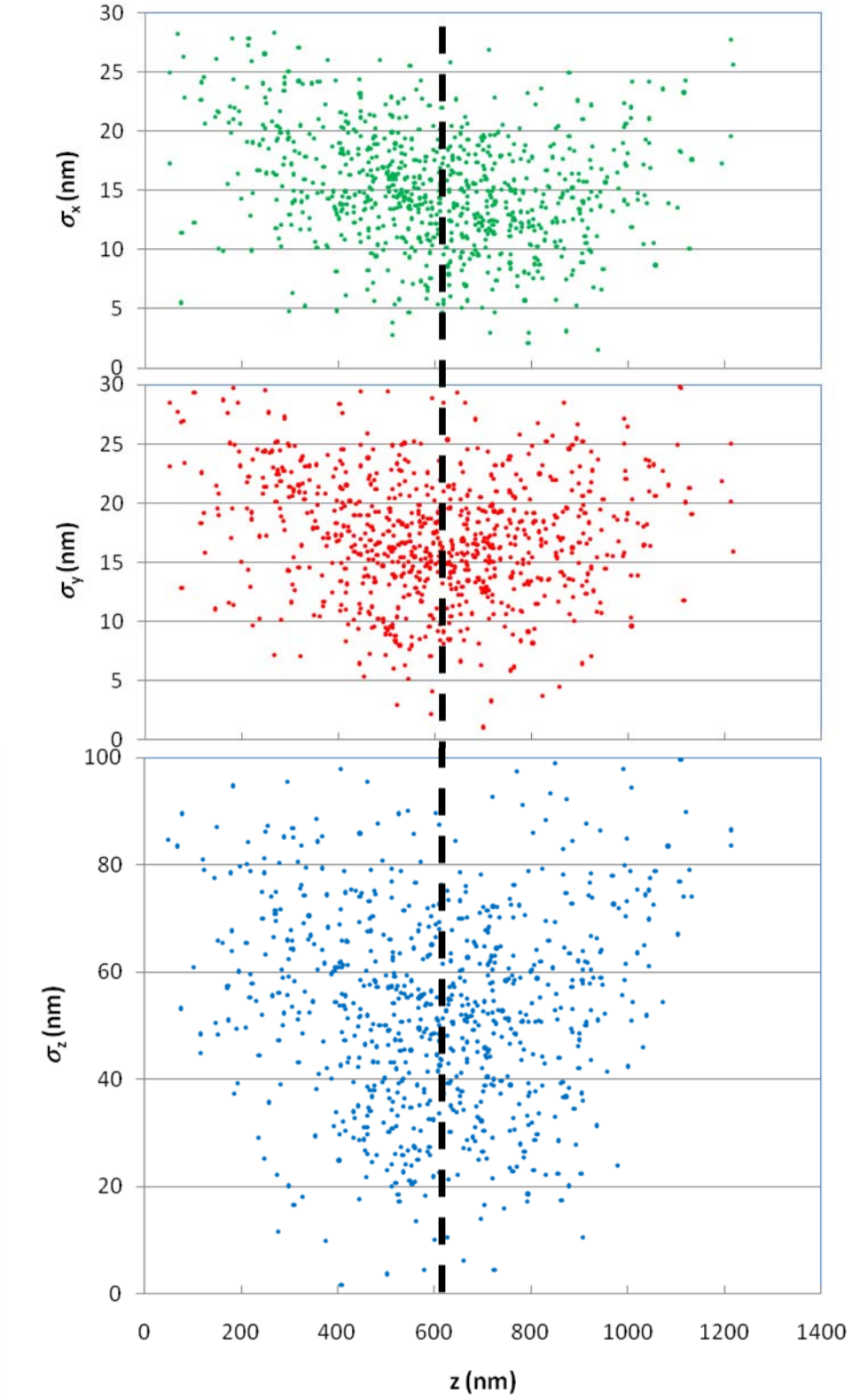

Figure S1 – Standard deviation of the measured *x*, *y*, and *z* positions, as a function of molecular depth, *z*. The dashed line indicates the focal plane at $z = 612$ nm.

Dynamics of the FtsZ-Dendra2 system

An interesting observation from bulk-level studies is that FtsZ is very dynamic *in vivo*, turning over rapidly.[7, 8] We therefore took advantage of the dynamic behavior of FtsZ for imaging.

As has been previously reported for other wide-field epifluorescence investigations of single molecules in live bacterial cells,[2, 9] when using EMCCD acquisition times greater than 5-10 ms, soluble (freely diffusing) molecules cannot be resolved as their emission signal is spread out over many camera pixels. Conversely, slower-moving molecules (such as polymerized proteins) are well-localized with acquisition times in the range 15-100 ms. In the current study, we imaged live cells expressing FtsZ-Dendra2 with a 15-ms frame rate to capture and localize only FtsZ molecules that had been incorporated into the midplane ring. On the other hand, all molecules in fixed cells are immobilized and therefore resolvable regardless of acquisition time. Consistently, the fixed sample showed localizations both within and away from the midplane ring.

In addition to photoswitching based on 407-nm laser irradiation of the Dendra2 protein, the live-cell samples benefited from the FtsZ dynamics for imaging more molecular positions. After each 407-nm pulse, our cells contained 10-100 FtsZ-Dendra2 fusion proteins, but only 1-2 labeled FtsZ molecules were incorporated into the Z-ring at a given time. Due to the fast dynamics of FtsZ, these molecules depolymerized and were rendered undetectable within a few imaging frames, only to be replaced by a novel sparse subset of fluorescently labeled proteins. As a result, a large number of single FtsZ-Dendra2 molecules were imaged and localized after each 407-nm photoswitching laser pulse. This can be viewed as repetitive sampling of the possible FtsZ positions in the ring.

The improvement in ability to resolve the FtsZ midplane ring using dynamics in live cells is further illustrated in Figures S2-S5. As opposed to the super-resolution reconstructions in Figures 3-6 in the main text, in Figures S2-S5, each localization is depicted by a single point and the color and size of that point indicates the fit error (darker and bigger indicates higher confidence in the fit). In the live cells (Figures S2 and S3, corresponding to Figures 3 and 4 of the main text, respectively), few localizations were obtained outside of the FtsZ midplane superstructure (ring or focus), and the localizations that are outside this superstructure are less precise (consistent with freely moving cytoplasmic proteins). In the fixed cells (Figures S4 and S5, corresponding to Figures 5 and 6 of the main text, respectively), there are more localizations outside of the midplane superstructure, and these molecules are as well localized (as dark) as their counterparts in the superstructure. Additionally, for a similar imaging time, more localization events are observed in the live cells than the fixed cells because more photoswitching was needed in the fixed cells.

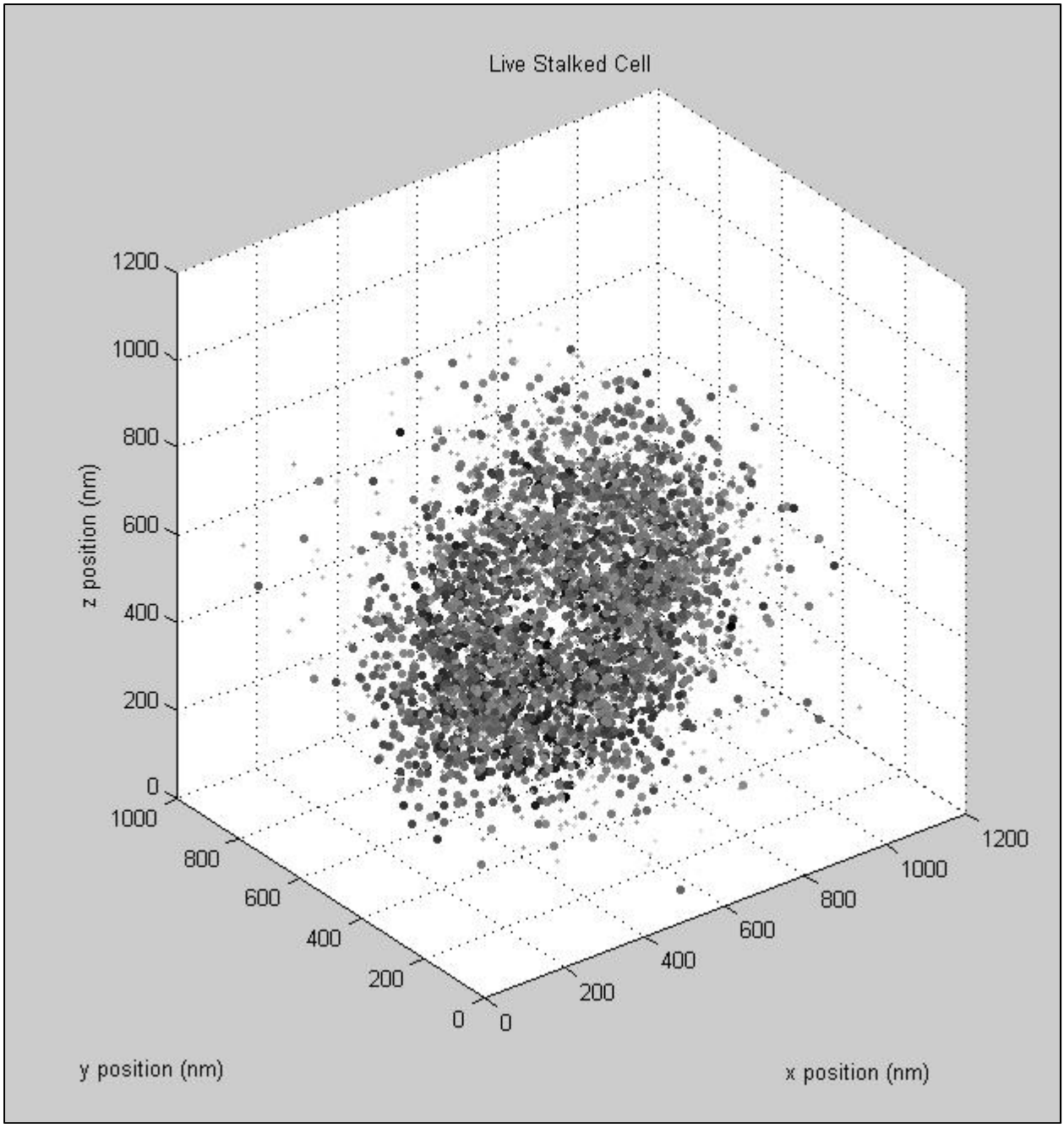

Figure S2. Scatter plot showing all of the localizations obtained for the live stalked cell composite in Figure 3. The size and darkness of each dot is proportional to the number of photons detected for that localization event, and therefore to the localization accuracy.

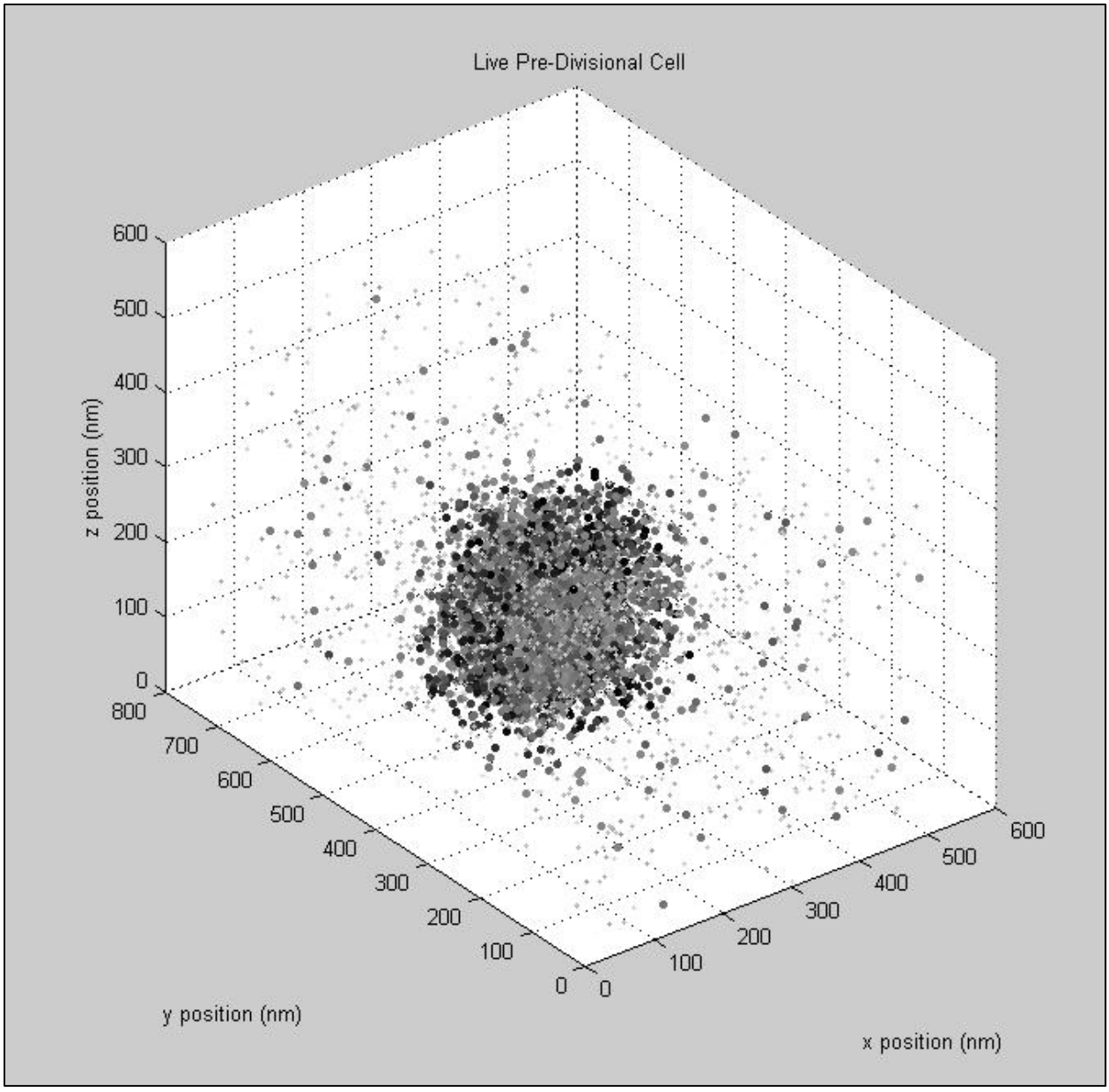

Figure S3. Scatter plot showing all of the localizations obtained for the live pre-divisional cell composite in Figure 4. The size and darkness of each dot is proportional to the number of photons detected for that localization event, and therefore to the localization accuracy.

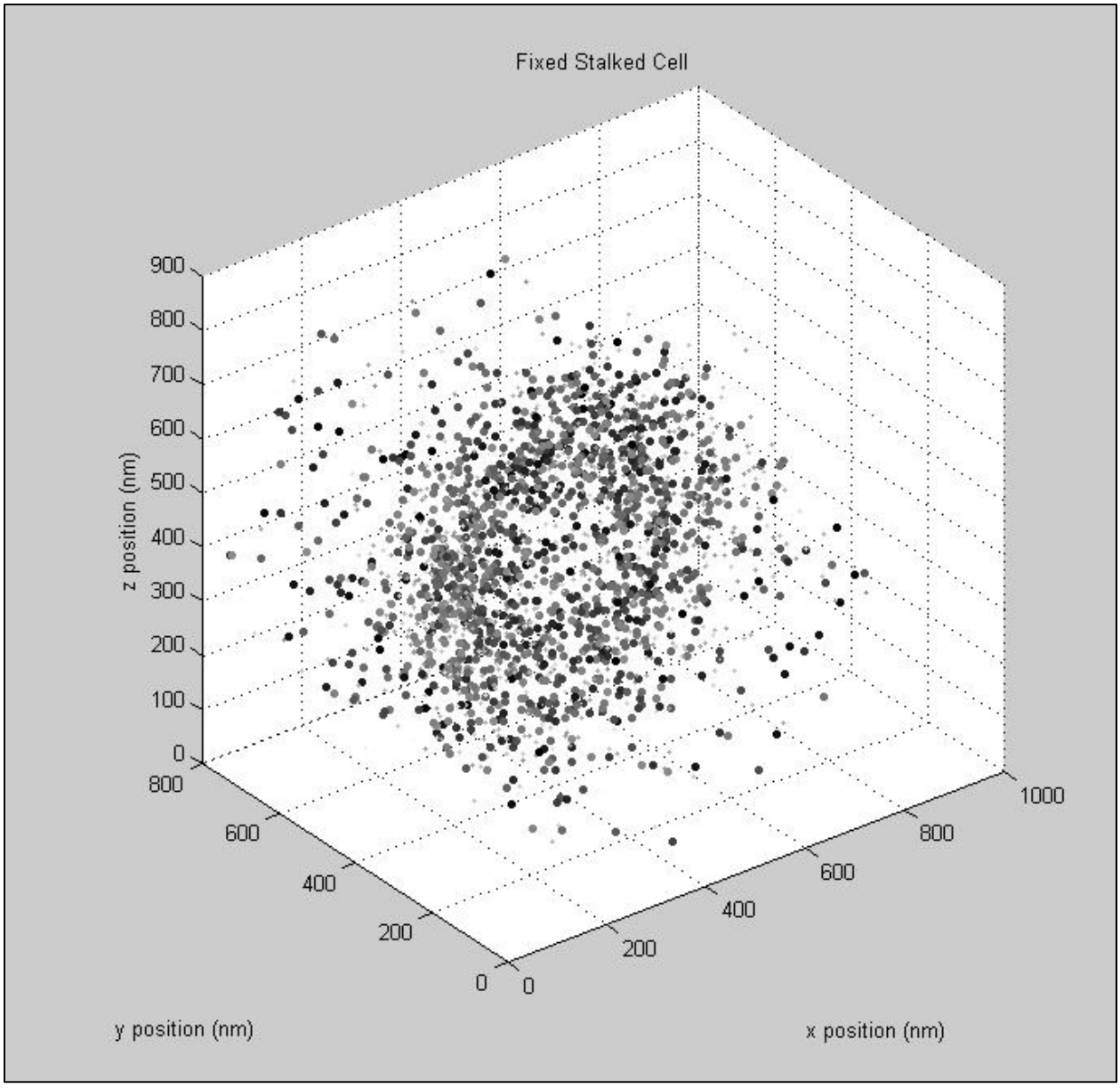

Figure S4. Scatter plot showing all of the localizations obtained for the fixed stalked cell composite in Figure 5. The size and darkness of each dot is proportional to the number of photons detected for that localization event, and therefore to the localization accuracy.

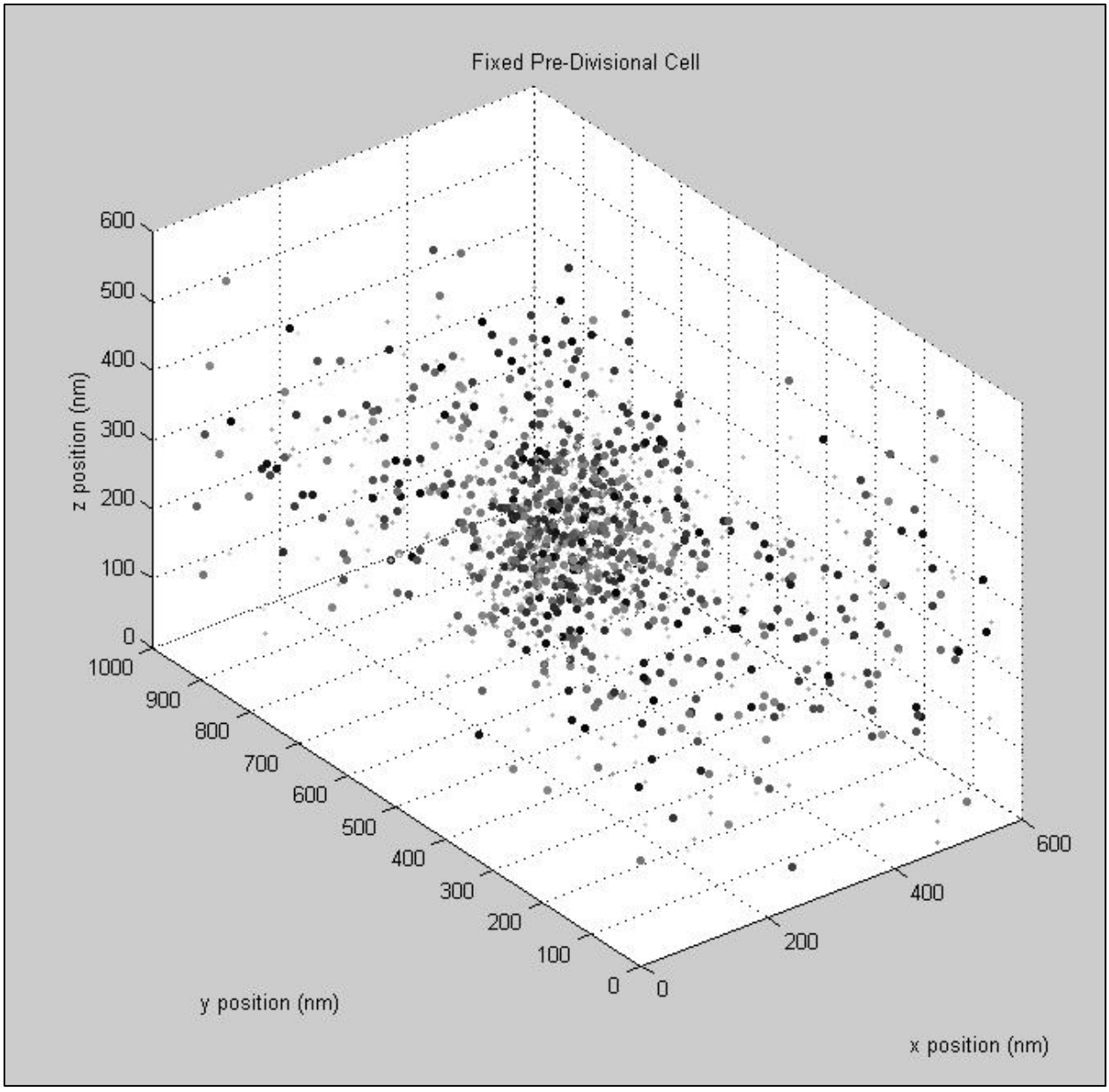

Figure S5. Scatter plot showing all of the localizations obtained for the fixed pre-divisional cell composite in Figure 6. The size and darkness of each dot is proportional to the number of photons detected for that localization event, and therefore to the localization accuracy.

Characterizing the FtsZ midplane Z-ring by super-resolution microscopy

The live-cell single-molecule images of FtsZ-Dendra2 can be used to determine the size of the FtsZ midplane ring in the cells. A typical stalked cell reconstruction (red box in Figure 2 of the main text) is shown in Figure S6A. This is a view of the FtsZ ring in a stalked cell projected along the *z* axis. The ring spans the entire width of the cell in which it is found, and the ring thickness is found to be 69 nm Figure S6C). This is consistent with the model of many overlapping filaments.[10] A typical pre-divisional cell reconstruction (blue box in Figure 2 of the main text) is shown in Figure S6B. This is a view of the polymerized FtsZ projected along the *z* axis. Here, instead of a thin line, a small focus is observed that is symmetric along the longitudinal and lateral axes of the cell and has a width of 86 nm (Figure S6D); greater than the width of the stalked cell ring.

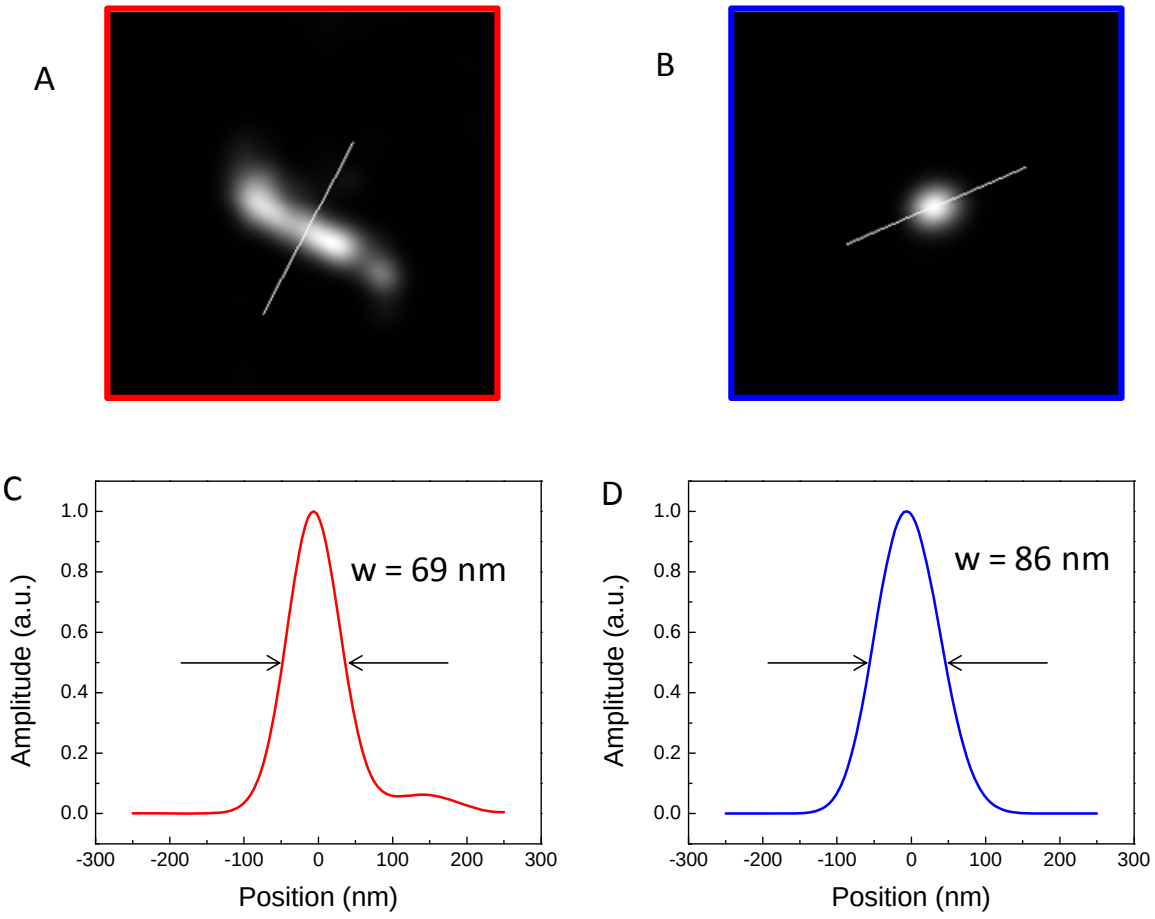

Figure S6. Investigations of the stalked and pre-divisional cells highlighted in Figure 2. (A) 1 μm by 1μm region of Figure 1 showing the stripe structure typically observed in stalk cells, (B) 1 μm by 1μm region of Figure 2 showing the punctate structure typically observed in dividing cells. (C) cross section of data in A along the grey line; this data is well fit by a Gaussian of width 69 nm. (D) cross section of data in A along the grey line; this data is well fit by a Gaussian of width 86 nm.

Supporting References

[1] W. E. Moerner, D. P. Fromm, *Rev. Sci. Instrum.* **2003**, *74*, 3597-3619.

[2] J. S. Biteen, M. A. Thompson, N. K. Tselentis, G. R. Bowman, L. Shapiro, W. E. Moerner, *Nat. Methods* **2008**, *5*, 947-949.

[3] N. G. Gurskaya, V. V. Verkhusha, A. S. Shcheglov, D. B. Staroverov, T. V. Chepurnykh, A. F. Fradkov, S. Lukyanov, K. A. Lukyanov, *Nat Biotech* **2006**, *24*, 461-465.

[4] B. Huang, W. Wang, M. Bates, X. Zhuang, *Science* **2008**, *319*, 810-813.

[5] Y. Deng, J. W. Shaevitz, *Appl. Opt.* **2009**, *48*, 1886-1890.

[6] M. Badieirostami, M. D. Lew, M. A. Thompson, W. E. Moerner, *Appl. Phys. Lett.* **2010**, *97*, 161103.

[7] J. Stricker, P. Maddox, E. D. Salmon, H. P. Erickson, *Proc. Natl. Acad. Sci. USA* **2002**, *99*, 3171-3175.

[8] D. E. Anderson, F. J. Guieros-Filho, H. P. Erickson, *J. Bacteriol.* **2004**, *186*, 5775-5781.

[9] S. Y. Kim, Z. Gitai, A. Kinkhabwala, L. Shapiro, W. E. Moerner, *Proc. Nat. Acad. Sci. U. S. A.* **2006**, *103*, 10929-10934.

[10] H. P. Erickson, D. E. Anderson, M. Osawa, *Microbiol. Mol. Biol. Rev.* **2010**, *74*, 504-528.